Magnetic Cooling at a Single Molecule Level: a Spectroscopic Investigation of Isolated Molecules on a Surface

*Valdis Corradini, Alberto Ghirri, Andrea Candini, Roberto Biagi, Umberto del Pennino, Gianluca Dotti, Edwige Otero, Fadi Choueikani, Robin J. Blagg, Eric J. L. McInnes, and Marco Affronte**

Magnetic cooling relies on a large entropy variation of magnetic systems under the application of an external magnetic field. While the giant magnetocaloric effect (MCE) in intermetallic compounds is related to the interplay between long range magnetic and lattice order, molecular nanomagnets have recently shown superior cooling performances at cryogenic temperatures. The molecular cage[1] $Fe_{14}(bta)_6$ (Hbta = benzotriazole) was one of the first examples for which enhanced MCE was experimentally observed in bulk samples[2,3] followed by a dozen of other cases[4–9] in recent years. Analysis of the low temperature thermodynamic properties of these molecular compounds shows that a large part of the entropy variation is due to the magnetic degeneracy of the ground molecular state and, therefore, high cooling power is expected at a single molecule level, an interesting feature that can be exploited for applications down to the nanometer scale. However, several investigations have shown that the deposition of large molecular cages on surfaces might be a non-innocent process since the interaction with the surface may provoke, in some cases, drastic chemical changes[10–13] or structural distortions that may alter the magnetic features[14–19] and, therefore, the functionalities of the molecule. All this instilled curiosity to check whether the functionality of potential molecular coolers is preserved when molecules are deposited on a substrate.

Here we report an investigation of a $Fe_{14}(bta)_6$ molecular nanomagnet to demonstrate that a large MCE is a property held at the single molecule level. To this end we characterize well isolated $Fe_{14}(bta)_6$ molecules deposited on a gold surface from a liquid phase by a combined surface analysis carried out using scanning tunneling microscopy (STM), X-ray photoemission (XPS) and absorption spectroscopies (XAS), and X-ray magnetic circular dichroism (XMCD) to independently check the chemical and magnetic features of isolated molecules.

The synthesis and characterization of the molecular derivative $Fe_{14}(bta)_6O_6(OMe)_{18}Cl_6$ ($Fe_{14}(bta)_6$ in short) studied in this work have been previously reported,[1,20] see **Figure 1**b. $Fe_{14}(bta)_6$ is soluble in dichloromethane (DCM) thus we used a liquid phase method to deposit it on substrates. The Au(111) surface was immersed for 10 min in a 10^{-4} M solution in DCM, rinsed for 20 s in DCM, and blow dried in a flux of nitrogen gas. In this way a uniform sub-monolayer (sub-ML) of isolated $Fe_{14}(bta)_6$ molecules is obtained (Figure 1) as evidenced by STM and XPS. From a statistical analysis of the STM images we derived that about 25–35% of the surface was occupied by $Fe_{14}(bta)_6$ clusters.

STM images (Figure 1a) show no aggregation of the molecules that, for the concentration we used, are well separated from each other and in direct contact with the gold surface. The low level of noise and the stability of the clusters even at high tunneling currents confirm the strength of the grafting of the molecule to the Au surface simply by van der Waals interactions. From the STM line profiles (Figure 1a), we reproducibly derive a diameter of 1.3 ± 0.5 nm and a height of 0.3 ± 0.1 nm in agreement with the dimensions of a single $Fe_{14}(bta)_6$ molecule as determined by structural crystallographic analysis (Figure 1b). As expected from the symmetric shape of this molecule, no preferential orientation is observed in the STM images.

The STM results are confirmed by quantitative XPS investigations. In Figure S1 (see Supporting Information) the Fe 2p, N 1s, Cl 2p, and O 1s core level line-shapes of the $Fe_{14}(bta)_6$ sub-ML on a Au(111) surface fit well to the corresponding spectra obtained for a thick film (TF) on the same substrate (see Experimental section for details). The stoichiometric ratios are well reproducible (Cl/(14Fe) = 6.1 ± 0.5, N/(14Fe) = 17.6 ± 0.5, and O/(14Fe) = 25 ± 4) and close to the expected ones (6, 18, and 24, respectively), proving the chemical integrity of the molecular core, in particular, the stability of the six atoms (O, Cl, and N) of the Fe octahedron. Due to the deposition protocol (use of solvent, exposure to ambient), we cannot exclude that some methyl groups are partially lost from the external

Dr. V. Corradini, Dr. A. Ghirri, Dr. A. Candini,
Dr. R. Biagi, Prof. U. del Pennino, Prof. M. Affronte
S3 Centre, Institute Nanoscience - CNR,
via G. Campi 213/A, 41125 Modena, Italy
E-mail: marco.affronte@unimore.it
Dr. E. Otero, Dr. F. Choueikani
Synchrotron SOLEIL, L'Orme des Merisiers
91120 Saint-Aubin, France
Dr. R. J. Blagg, Prof. E. J. L. McInnes
School of Chemistry and Photon Science Institute
University of Manchester
Oxford Road, Manchester, M13 9PL, UK
Dr. R. Biagi, Prof. U. del Pennino, G. Dotti, Prof. M. Affronte
Dipartimento di Scienze Fisiche
Informatiche e Matematiche
Università di Modena e Reggio Emilia
via G. Campi 213/A, 41125 Modena, Italy

DOI: 10.1002/adma.201205257

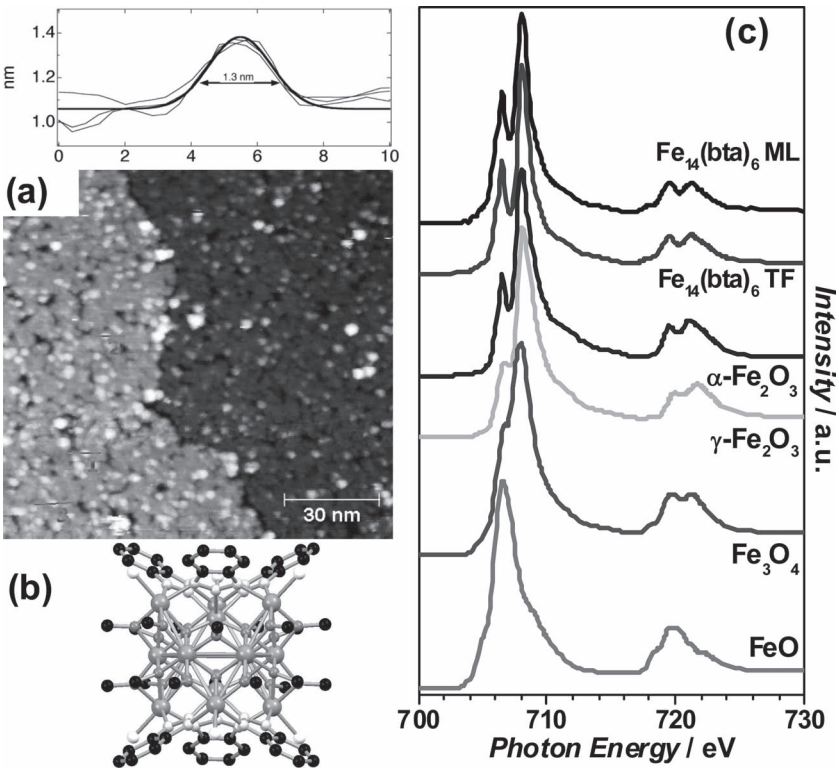

Figure 1. a) STM image (2.0 V, 30 pA) of a sub-ML of $Fe_{14}(bta)_6$ deposited on a Au(111) surface and line profiles (upper panel) taken along the directions indicated in (a). b) Molecular structure of the $Fe_{14}(bta)_6$ cluster. c) Fe $L_{2,3}$ XAS spectra for a $Fe_{14}(bta)_6$ sub-ML on Au(111) and the corresponding thick film (TF) compared with α-Fe_2O_3[21] where (Fe^{3+}, O_h), γ-Fe_2O_3[22] where (Fe^{3+}, O_h+T_d), Fe_3O_4[21] where (2/3Fe^{3+} + 1/3Fe^{2+}, O_h) and FeO[23] where (Fe^{2+}, O_h).

shell but without altering the stability of the six atoms (Cl, N, and O) which form the Fe octahedron. However, both STM and XPS analysis make us confident about the chemical and structural integrity of the $Fe_{14}(bta)_6$ as individual units, at least for what concerns the metallorganic core. To further check the integrity of the metal core of the molecule, we compared the Fe $L_{2,3}$ XAS spectrum collected for the $Fe_{14}(bta)_6$ sub-ML on Au(111) and the corresponding one obtained for a TF deposited on the same substrate with others reported in the literature for different Fe oxides (see Figure 1c). The XAS spectrum of the $Fe_{14}(bta)$ sub-ML is consistent with that obtained for the TF and with what is reported for α-Fe_2O_3[21] for which it is well established that Fe^{3+} ions are coordinated in O_h symmetry. Conversely, the observed XAS spectrum for the $Fe_{14}(bta)_6$ sub-ML differs from that reported for γ-Fe_2O_3, where Fe^{3+} ions are in O_h+T_d symmetry,[22] and for Fe_3O_4, where part (1/3) of the Fe ions are in the divalent state,[21] and for FeO where all Fe^{2+} ions are divalent and in O_h symmetry.[23] We conclude that in both the $Fe_{14}(bta)_6$ sub-ML and TF the iron ions are Fe^{3+} in O_h symmetry as expected from the crystallographic analysis, thus confirming that the interaction with the gold surface does not affect the valence electronic structure of the $Fe_{14}(bta)_6$ core: namely, the oxidation state and the crystal-field at the Fe sites are preserved.

Figure 2 shows the Fe $L_{2,3}$ absorption spectra taken using both photon helicities (upper panels) with the relative dichroic signal (lower panels) measured at 4 K and 6 T for the sub-ML of $Fe_{14}(bta)_6$ on Au(111) (on the right) and for the TF (on the left). The dichroic XMCD signal (%) can be evaluated taking the difference between the two XAS spectra obtained with the different X-ray polarizations ($\sigma^{\uparrow\downarrow} - \sigma^{\uparrow\uparrow}$) and dividing by the average height of the L_3 edge (see Experimental section for details). While the shape of both the XAS and XMCD spectra are essentially identical for the TF and sub-ML, the relative intensities of the XMCD signal are different. Note that this XMCD value expressed in percentage is independent of the amount of the derivative analyzed, thus the signal on sub-ML can be directly compared with that obtained on TF although the interpretation and quantification of the dichroic signal in terms of absolute magnetic moments is not straightforward. We proceed as follows.

According to what is reported in the literature[24,25] for Fe^{3+} ions in octahedral symmetry O_h, we assume that the XMCD curve is simply proportional to the magnetization if the shape of the spectrum remains unchanged. We checked – although not shown in the figure – that the shape of the dichroic signal does not change with temperature and magnetic field. Thus we obtained a fast detection of the dichroic signal by simply measuring the edge (E) and pre-edge (P) intensities $2[(E\sigma^{\uparrow\downarrow} - P\sigma^{\uparrow\downarrow}) - (E\sigma^{\uparrow\uparrow} - P\sigma^{\uparrow\uparrow})]/[(E\sigma^{\uparrow\downarrow} - P\sigma^{\uparrow\downarrow}) + (E\sigma^{\uparrow\uparrow} - P\sigma^{\uparrow\uparrow})]$ (see Figure 2) when the magnetic field was swept under isothermal conditions.

In **Figure 3** (upper panel) we report the dichroic signal (%) as a function of the applied magnetic field (up to 6 T), at different temperatures (from 4 to 20 K) measured on the $Fe_{14}(bta)_6$ TF and we compare this with the magnetization $M(H)$ measured on a bulk sample (for sake of clarity we report only the curve at 20 K, from Evangelisti et al.[2]). We observe that the dependence of the XMCD signal on the magnetic field follows quite closely that of the bulk magnetization, validating our interpretation of the dichroic signal in terms of magnetization and allowing us to find the numerical factor relating the magnetization with the intensity of the dichroic signal. With the same procedure, we evaluated the magnetization dichroic signal (%) for a sub-ML of isolated $Fe_{14}(bta)_6$ on the Au surface and we plotted it as a function of magnetic field for different temperatures (Figure 3, lower panel). The behavior of isolated molecules (sub-ML) is clearly different from that observed for the TF. If we take two curves at corresponding temperatures we indeed notice that the saturation value of the dichroic signal is smaller for the sub-ML than for the TF.

In order to provide more quantitative information we now explicitly refer to the XMCD sum rules for of the determination of the magnetic moments (see Figure 2). According to these rules the average values of the spin (m_S) and orbital (m_O) moments (along the z direction) are given by:[26]

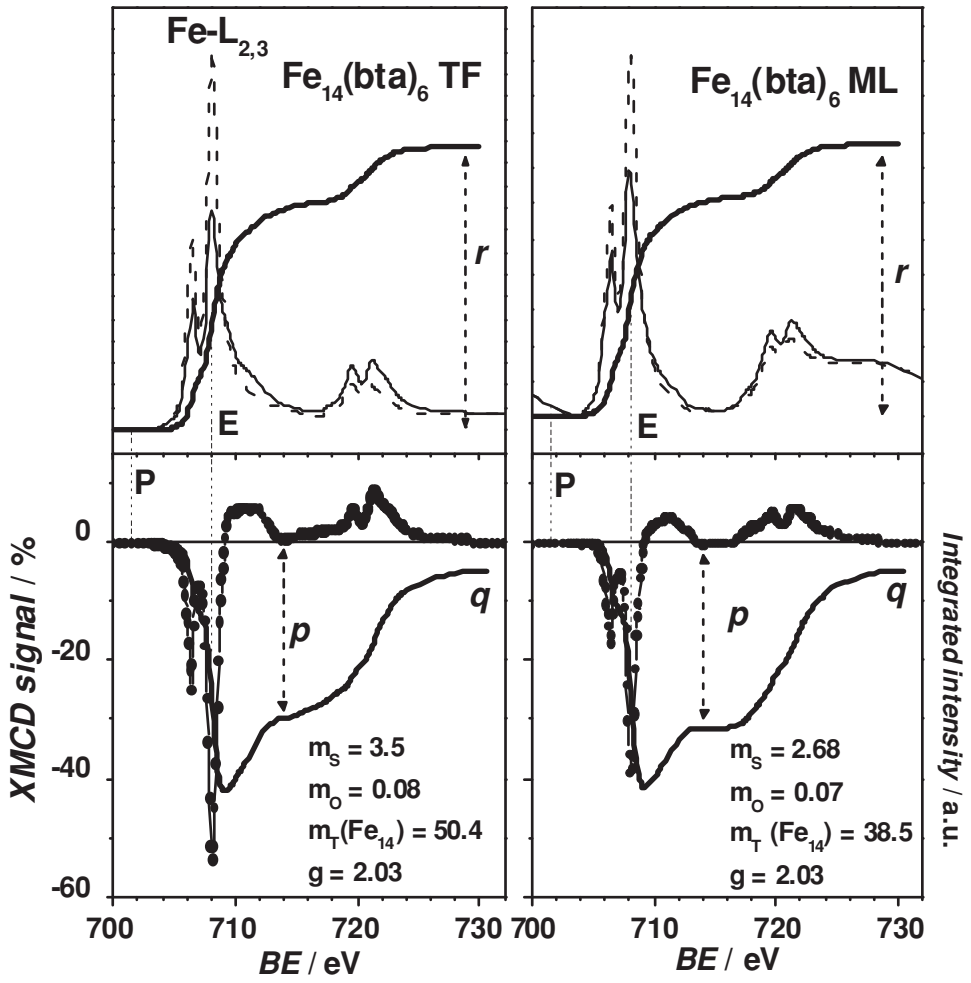

Figure 2. Upper panels: Fe $L_{2,3}$ XAS spectra taken with $\sigma^{\uparrow\uparrow}$ and $\sigma^{\uparrow\downarrow}$ circularly polarized light at 4 K, 6 T and the XAS integral (thick lines) for the $Fe_{14}(bta)_6$ TF (left panels) and the sub-ML on Au(111) (right panels). Lower panels: XMCD ($\sigma^{\uparrow\downarrow} - \sigma^{\uparrow\uparrow}$) spectra (lines and dots) and their integrals (thick lines). E and P represent the edge and pre-edge positions. *p* and *q* are the values of the integrals used for the sum rules analysis. Parameters indicated in figure are those obtained by the application of isotropic sum rules with $T_z = 0$ and $S_c = 1.8$.

$$\frac{m_o}{\mu_B} = -\frac{4q \cdot N_{eff}}{3r}$$

$$\frac{m_S}{\mu_B} = -\frac{(6p - 4q) \cdot N_{eff}}{r} \cdot S_C + \frac{7\langle T_Z \rangle}{\mu_B}$$

where *r* is the integral of the white line, $p = A$ and $q = A + B$, where *A* and *B* are the integrals of the dichroic signal at the L_3 and L_2 edges, respectively. The applicability of the isotropic ($T_z = 0$) sum rules for Fe^{3+} ions in octahedral symmetry has already been predicted in the literature[24,25] and for our specific case a detailed argument is presented in the Supporting Information. In order to obtain a full quantitative agreement between the XMCD and the bulk magnetization we use a spin correction factor (S_C) accounting for the partial *j*–*j* mixing of 1.8 that is quite close to the value of 1.5 reported in the literature for O_h Fe^{3+} (10 Dq = 1.5 eV).[24] The *q* value of the dichroic signal at the Fe $L_{2,3}$ edges is related to the orbital moment m_O of the Fe^{3+} ions. The vanishing of its value indicates a quite complete quenching of m_O due to crystal field in both the TF and the sub-ML. This implies that in both systems Fe^{3+} ions have essentially only a spin moment m_S and a nearly spin-only gyromagnetic factor ($g = 2.03$). Thus the interaction with the Au surface does not affect the degree of quenching of the orbital momentum. This quantitative analysis confirms that the magnetization curve of the sub-ML tends to saturate at a value ≤ 40 μ_B molecule^{-1} indicating a ground state of the isolated molecules, in applied magnetic fields, of S ≤ 20 while for the bulk we have the saturation of magnetization at $M_S = 50$ μ_B molecule^{-1} which, instead, points to a ground state close to S = 25.[2] This change in the magnetic features of $Fe_{14}(bta)_6$ is not astonishing since a simple magnetochemical analysis reveals the presence of many states with similar low energy but different spin values as already evidenced by early magnetization measurements on the bulk.[1] Assuming a simple spin model with two *J* constants to account for a different type of Fe…Fe interactions within the $Fe_{14}(bta)_6$ cage, we have that states with different molecular spin actually co-exist within a small energy range

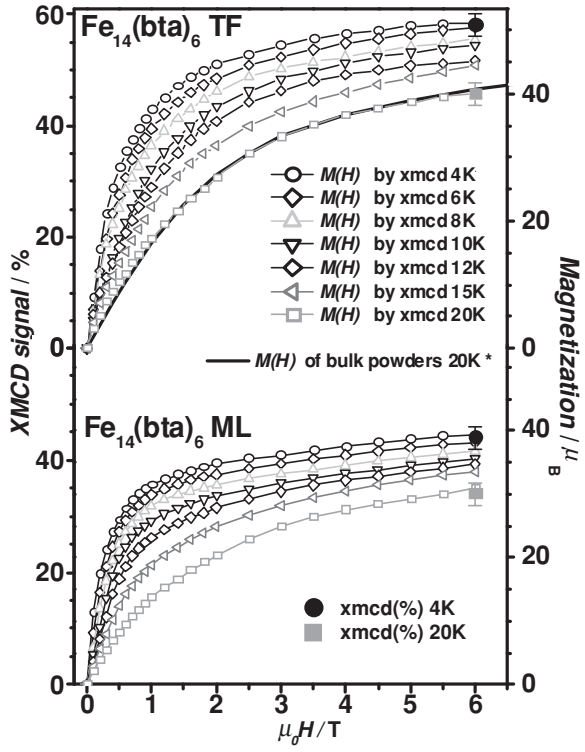

Figure 3. Isothermal *M*(*H*) curves derived by the XMCD signal measured as a function of field (open symbols) at different *T* (from 4 to 20 K) for a $Fe_{14}(bta)_6$ TF (upper panel) and for a sub-ML on Au(111) (lower panel). (*) Magnetization curve measured on bulk microcrystalline powders at 20 K (continuous line) taken from Evangelisti et al.[2] Values of the XMCD signal (%) and corresponding magnetic moment derived by the sum rules in μ_B (see the *y*-axis on the right) measured at 4 K, 6 T (filled circles) and 20 K, 6 T (filled squares).

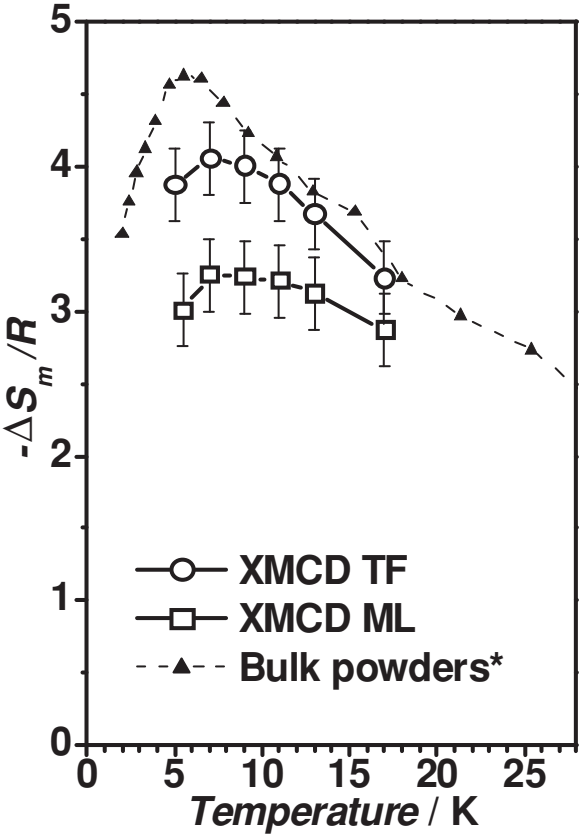

Figure 4. Entropy change ΔS_m vs *T* calculated for Hf $\mu 0 = 6$ T and Hi $\mu 0 = 0$ T, derived from the isothermal *M(H)* curves of **Figure 3** for the TF and the sub-ML compared with bulk microcrystalline powders taken from Evangelisti et al.[2]

and, by slight changes of the *J'*/*J* ratio, the ground state can actually span from 19 to 25.[1,27,28] Thus, we ascribe the change in the magnetization to a small distortion of the Fe cage and/or to the interaction of the isolated $Fe_{14}(bta)_6$ molecule with the gold surface. Based on the magnetization curves reported in Figure 3a and Figure 3b and assuming that the dichroic signal is proportional to the absolute value of the magnetization, as established in the discussion above, we can now estimate the entropy change ΔS_m between different magnetic fields at different temperatures by using conventional Maxwell equations:

$$\Delta S_m(T)_{\Delta H} = \int_{H_i}^{H_f} \left[\frac{\partial M(T, H)}{\partial T}\right]_H dH \quad (1)$$

Results for both TF and sub-ML are plotted in **Figure 4** for $H_f \mu_0 = 6$ T and $H_i \mu_0 = 0$ T and they are compared with similar results obtained for the crystalline bulk sample from Evangelisti et al.[2] It turns out that ΔS_m for TF is close to that measured in the bulk sample while in the sub-ML ΔS_m is significantly smaller (35%) than in the bulk. In both TF and sub-ML the maximum of ΔS_m vs *T* is less evident than in the bulk also due to the limited number of experimental data available at low temperature. To interpret these results it is worth remembering that the entropy variation in crystalline $Fe_{14}(bta)_6$ is given by a combination of the degeneracy removal at a single molecule level and the cooperative behavior. Indeed crystalline $Fe_{14}(bta)_6$ undergoes a long range (antiferro-)magnetic transition at low temperature and this certainly contributes to ΔS_m in the crystal but probably not in a disordered TF (and sub-ML). A further reduction of the absolute value of ΔS_m in the sub-ML is given by the reduced degeneracy of the ground state with a smaller *S* number in the zero field. In spite of this the absolute value of ΔS_m is still considerable since ΔS_m achieves its maximum of 13 J $kg^{-1}K^{-1}$ at 7 K, that is much larger than that of single ions. The relevant point is that the MCE is directly observed in our experiments at a single molecule level. This demonstrates, for the first time, that an important contribution to magnetic refrigeration is an intrinsic molecular property and it opens the possibility of scaling cooling devices down to a molecular level with no need of a cooperative (magnetic and or reticular) behavior.

Experimental Section

The sub-MLs were obtained by immersing for 10 min a Au(111) single crystal or a Au/mica flame-annealed surface in a 10^{-4} M solution of

$Fe_{14}(bta)_6$ using DCM as solvent, rinsed for 20 s in DCM, and blow dried in a flux of nitrogen gas. TFs were obtained by drop casting the saturated solution on the same substrates. STM and XPS were used to check that the desired two dimensional distribution of nanometric entities had been actually obtained. The tips used were electrochemically etched tungsten wires. Room temperature STM acquisitions were carried out in constant current mode with typical imaging conditions of 2.0 V and the lowest achievable current (30 pA) in order to minimize dragging and damaging the soft organic materials by the scanning tip. XPS measurements were performed using an Omicron hemispherical analyzer (EA125) and a non-monochromatized Mg Kα X-ray source ($h\nu = 1253.6$ eV).

Soft XAS and XMCD measurements were performed at the DEIMOS beamline of the SOLEIL Synchrotron Radiation Facility (France). The lowest sample temperature reached was about 4 K and the base pressure of the experimental chamber was 1.0×10^{-10} mbar. Attention was paid to avoid any sample degradation induced by radiation exposure, working at very low flux (below 10^{10} photons s^{-1}) and by strictly monitoring the XAS spectra throughout all the experiments to detect even the smallest traces of sample damage. XMCD measurements at the Fe $L_{2,3}$ edges were performed in total electron yield mode using circularly polarized light with an ~100% polarization rate and with external magnetic field $\mu_0 H$ up to 6 T applied perpendicularly to the sample surface and parallel to the incident photon beam. The dichroic spectrum is the difference between the XAS spectra taken with the helicity of the incident photon antiparallel ($\sigma^{\uparrow\downarrow}$) and parallel ($\sigma^{\uparrow\uparrow}$) to the applied magnetic field (H). In order to minimize the effects of field inhomogeneity, we carried out measurements by switching both the helicities and the applied field. The $\sigma^{\uparrow\uparrow}$ ($\sigma^{\uparrow\downarrow}$) absorption spectra are, therefore, the average spectra collected with the helicity parallel (antiparallel) to H.

Supporting Information

Supporting Information is available from the Wiley Online Library or from the author.

Acknowledgements

The XAS and XMCD measurements were performed at the DEIMOS beamline, using the Chemistry 1 support laboratory, at SOLEIL Synchrotron. The MBE chamber used during the beamtime on DEIMOS has been funded by the Agence National de la Recherche; grant ANR-05-NANO-073. The authors are grateful to Philippe Ohresser and to DEIMOS staff for assistance and to the SOLEIL staff for smoothly running the facility. This work was partially funded by EPSRC in UK.

Received: December 21, 2012
Revised: February 1, 2013
Published online: April 12, 2013

[1] D. M. Low, L. F. Jones, A. Bell, E. K. Brechin, T. Mallah, E. Rivière, S. J. Teat, E. J. L. McInnes, *Angew. Chem. Int. Ed.* **2003**, *42*, 3781.
[2] M. Evangelisti, A. Candini, A. Ghirri, M. Affronte, E. K. Brechin, E. J. L. McInnes, *Appl. Phys. Lett.* **2005**, *87*, 072504.
[3] M. Affronte, A. Ghirri, S. Carretta, G. Amoretti, S. Piligkos, G. Timco, R. E. P. Winpenny, *Appl. Phys. Lett.* **2004**, *84*, 3468.
[4] M. Manioli, R. D. L. Johnstone, S. Parsons, M. Murrie, M. Affronte, M. Evangelisti, E. K. Brechin, *Angew. Chem. Int. Ed.* **2007**, *119*, 4540.
[5] J. W. Sharples, Y. Z. Zheng, F. Tuna, E. J. L. McInnes, D. Collison, *Chem. Commun.* **2011**, *47*, 7650.
[6] S. K. Langley, N. F. Chilton, B. Moubaraki, T. Hooper, E. K. Brechin, M. Evangelisti, K. S. Murray, *Chem. Sci.* **2011**, *2*, 1166.
[7] S. Dinca, A. Ghirri, A. M. Madalan, M. Affronte, M. Andruh, *Inorg. Chem.* **2012**, *51*, 3935.
[8] Y. Z. Zheng, M. Evangelisti, R. E. P. Winpenny, *Angew. Chem. Int. Ed.* **2011**, *50*, 3692.
[9] M. Evangelisti, O. Roubeau, E. Palacios, A. Camon, T. N. Hooper, E. K. Brechin, J. J. Alonso, *Angew. Chem. Int. Ed.* **2011**, *50*, 6606.
[10] A. Ghirri, V. Corradini, V. Bellini, R. Biagi, U. del Pennino, V. De Renzi, J. C. Cezar, C. A. Muryn, G. A. Timco, R. E. P. Winpenny, M. Affronte, *ACS Nano* **2011**, *5*, 7090.
[11] A. Ghirri, V. Corradini, C. Cervetti, A. Candini, U. del Pennino, G. Timco, R. J. Pritchard, C. A. Muryn, R. E. P. Winpenny, M. Affronte, *Adv. Funct. Mater.* **2010**, *20*, 1552.
[12] V. Corradini, A. Ghirri, U. del Pennino, R. Biagi, V. A. Milway, G. Timco, F. Tuna, R. E. P. Winpenny, M. Affronte, *Dalton Trans.* **2010**, *39*, 4928.
[13] F. Moro, V. Corradini, M. Evangelisti, V. De Renzi, R. Biagi, U. del Pennino, C. J. Milios, L. F. Jones, E. K. Brechin, *J. Phys. Chem. B* **2008**, *112*, 9729.
[14] F. Moro, R. Biagi, V. Corradini, M. Evangelisti, A. Gambardella, V. De Renzi, U. del Pennino, E. Coronado, A. Forment-Aliaga, F. M. Romero, *J. Phys. Chem. C* **2012**, *116*, 14936.
[15] V. Corradini, A. Ghirri, E. Garlatti, R. Biagi, V. De Renzi, U. del Pennino, V. Bellini, S. Carretta, P. Santini, G. Timco, R. E. P. Winpenny, M. Affronte, *Adv. Funct. Mater.* **2012**, *22*, 3706.
[16] V. Corradini, F. Moro, R. Biagi, V. De Renzi, U. del Pennino, V. Bellini, S. Carretta, P. Santini, V. A. Milway, G. Timco, R. E. P. Winpenny, M. Affronte, *Phys. Rev. B* **2009**, *79*, 144419.
[17] F. Moro, V. Corradini, M. Evangelisti, R. Biagi, V. De Renzi, U. del Pennino, J. C. Cezar, R. Inglis, C. J. Milios, E. K. Brechin, *Nanoscale* **2010**, *2*, 2698.
[18] R. Biagi, J. Fernandez-Rodriguez, M. Gonidec, A. Mirone, V. Corradini, F. Moro, V. De Renzi, U. del Pennino, J. C. Cezar, D. B. Amabilino, J. Veciana, *Phys. Rev. B.* **2010**, *82*, 224406.
[19] M. Gonidec, R. Biagi, V. Corradini, F. Moro, V. De Renzi, U. del Pennino, D. Summa, L. Muccioli, C. Zannoni, D. B. Amabilino, J. Veciana, *J. Am. Chem. Soc.* **2011**, *133*, 6603.
[20] R. S. Shaw, R. H. Laye, L. F. Jones, D. M. Low, C. Talbot-Eeckelaers, Q. Wei, C. J. Milios, S. Teat, M. Helliwell, J. Raftery, M. Evangelisti, M. Affronte, D. Collison, E. K. Brechin E. J. L. McInnes, *Inorg. Chem.* **2007**, *46*, 4968.
[21] K. Kuepper, I. Balasz, H. Hesse, A. Winiarski, K. C. Prince, M. Matteucci, D. Wett, R. Szargan, E. Burzo, M. Neumann, *Phys. Status Solidi A* **2004**, *201*, 3252.
[22] D. H. Kim, H. J. Lee, G. Kim, Y. S. Koo, J. H. Jung, H. J. Shin, J.-Y. Kim, J.-S. Kang, *Phys. Rev. B* **2009**, *79*, 033402.
[23] H. J. Lee, G. Kim, D. H. Kim, J.-S. Kang, C. L. Zhang, S.-W Cheong, J. H. Shim, Soonchil Lee, Hangil Lee, J.-Y. Kim, B. H. Kim, B. I. Min, *J. Phys.: Condens. Matter* **2008**, *20*, 295203.
[24] Y. Teramura, A. Tanaka, B. Thole, T. Jo, *J. Phys. Soc. Jpn.* **1996**, *65*, 3056.
[25] J. P. Crocombette, B. T. Thole, F. Jollet, *J. Phys.: Condens. Matter* **1996**, *8*, 4095.
[26] C. T. Chen, Y. U. Idzerda, H. J. Lin, N. V. Smith, G. Meigs, E. Chaban, G. H. Ho, E. Pellegrin, F. Sette, *Phys. Rev. Lett.* **1995**, *75*, 152.
[27] E. Garlatti, S. Carretta, P. Santini, private communication.
[28] G. Rajaraman, J. Cano, E. K. Brechin, E. J. L. McInnes, *Chem. Commun.* **2004**, 1476.